JOURNAL OF CATALYSIS 58, 34–42 (1979)

Characterization of Nickel–Tungsten Mixed Oxides Supported on α-Alumina

J. C. CONESA, A. CORTES, J. MARTI, J. L. SEOANE, AND J. SORIA

Instituto de Catálisis y Petroleoquímica, C.S.I.C., Serrano 119, Madrid-6, Spain

Received December 5, 1977, revised August 1, 1978

In this work we studied a series of nickel and tungsten oxide mixtures supported on α-Al_2O_3 by X-ray diffraction, electron spin resonance, and by transmission and scanning electron microscopy, both before and after use in the oxidative dehydrogenation of ethylbenzene to styrene. The results indicate that nickel alone supported on α-Al_2O_3 is substantially reduced to Ni metal during the reaction, while tungsten oxide only suffers a small loss of lattice oxygen. Both oxides appear to be more stable toward reduction, for this particular catalytic system, in the catalyst samples containing mixtures of the two oxides. Tungsten trioxide and nickel tungstate, on the other hand, seem to be the species more catalytically active, and both of them show a better crystallization pattern when they are in the presence of nickel oxide and excess tungsten trioxide, respectively.

INTRODUCTION

The transition metal oxides and their mixtures with elements of groups IV B and V B of the periodic table are of great interest as selective oxidation catalysts for the production of formaldehyde, acrolein, phthalic and maleic anhydrides, acrylic acid, and other compounds (*1*).

For the particular case of binary mixtures it has been found that their activity and selectivity change with the atomic ratio of the metals present in the catalyst (*2*). However, Boutry *et al.* detected the formation of a well-defined chemical compound (*3*), the composition of which appears to correspond with the oxide ratio in the sample with greater activity.

Recently we studied the oxidative dehydrogenation of ethylbenzene to styrene (*4*) on a series of nickel and tungsten oxide mixtures supported on α-alumina, with a constant amount of active phase and different W/Ni atomic ratios. The results indicated maximum styrene formation for the samples with W/Ni ratios between 2 and 4 (Fig. 1). For the single oxides we found that the percentage of complete combustion was about 42 for NiO/α-Al_2O_3 ($CO_2/CO \simeq 5$ mole/mole), as opposed to 16% for WO_3/α-Al_2O_3 ($CO_2/CO \simeq 3.5$ mole/mole), thus confirming that nickel oxide preferentially activates the C–C bonds, with subsequent greater complete degradation of the reactant hydrocarbon to $CO + CO_2$.

In a previous paper (*5*) we partially analyzed the above series of fresh catalysts by magnetic susceptibility and X-ray diffraction, but did not reach a definite explanation about their catalytic behavior. In the present work we studied in more detail these nickel–tungsten supported oxides, both before and after use in the catalytic reaction, by X-ray diffraction, electron spin resonance, and by trans-

0021-9517/79/070034-09$02.00/0

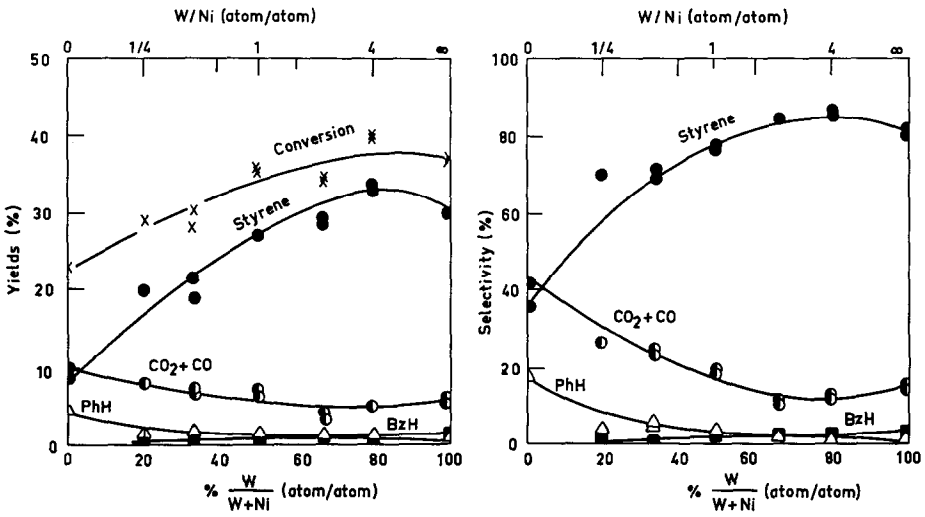

FIG. 1. Influence of the atomic ratio W/Ni on yields and selectivities [460°C; 20 g·sec/cm³; composition (vol%): O_2, 10; ethylbenzene, 10; N_2, 80].

mission and scanning electron microscopy, with the aim of getting a better insight into the physicochemical changes that may take place in the different catalyst samples, and their possible relationship with the catalytic properties of the samples.

EXPERIMENTAL METHODS

The preparation of the catalysts and the performance of the catalytic experiments have already been described in detail (*4*). The catalyst samples contain a constant amount of W + Ni (0.048 g atom/100 g α-Al_2O_3) and different W/Ni atomic ratios: 0, $\frac{1}{4}$, $\frac{1}{2}$, 1, 2, 4, and ∞.

The X-ray diffractograms were obtained with a Phillips PW 1051 powder diffractometer, using Cu*K* radiations at 40 kV and 20 mA, with slits of 1, 0.1, and 1°.

The ESR spectra were recorded in a Jeol JES-PE-3X apparatus, working in the X-band.

The transmission electron diagrams were obtained in an Elmiskop 102 microscope, of 100 kV, using a goniometer of double inclination and displacement.

Finally, the scanning electron micrographs were taken with a Philips PSEM 500 microscope, equipped with an energy dispersive X-ray analyzer (EDAX).

RESULTS AND DISCUSSION

X-ray Diffraction

The results of the X-ray analysis are summarized in Fig. 2, which contains the diffractograms of the spent catalysts with W/Ni ratios of ∞, 4, 2, and 0. The fresh samples gave essentially similar diffractograms, except for that with only nickel which is also included in the upper part of Fig. 2. In this figure we must consider that the α-Al_2O_3 support is a highly crystalline material which produces all the large peaks, and that the main peaks of NiO coincide with some of them. For the sake of clarity the α-Al_2O_3 peaks have been cut short.

In the sample containing only tungsten on alumina (W/Ni = ∞), the peaks are basically due to WO_3 in its low temperature form (monoclinic). If we compare, however, the values of 2θ and relative intensities with those of the pure WO_3 (Table 1), it seems that other crystallographic species may also be present; in particular, the high-temperature WO_3 (tetragonal) phase and possibly polymeric $W_{20}O_{58}$. Thus, in

TABLE 1

X-ray Diffraction: Angles (2θ) and Relative Intensities (I)

WO_3 (monoclinic)[a]		W/Ni = ∞		W/Ni = 4		W/Ni = 2	
2θ(°)	I	2θ(°)	I	2θ(°)	I	2θ(°)	I
23.17	100	23.2	90	23.1	100	23.3	90
23.63	95	23.6	100	23.6	79	23.8	79
24.42	100	24.2	57	24.3	84	24.5	100
33.35	75	33.4	48	33.3	45	33.4	47
34.25	90	34.1	38	34.1	47	34.4	63

[a] Other species to be considered are: high-temperature tetragonal WO_3 (2θ: *23.99 to 24.05*°; 33.06 to 33.17°; 52.99 to 55.34°); polymeric $W_{20}O_{58}$ (2θ: *23.54 to 23.59*°; 32.69 to 32.80°; 40.64 to 40.83°). Data taken from X-ray ASTM-1 data file.

Fig. 2 we can see another peak at 24.00°, a shoulder at about 33.35°, and a small peak around 55°, which could justify the presence of high-temperature tetragonal WO_3. As to the $W_{20}O_{58}$ species we can notice that its major peak (23.54 to 23.59°) may contribute to the one at 23.60° which is the largest in our sample not due to the support.

In the catalyst with W/Ni = 4 the major peaks again correspond to the low-temperature monoclinic WO_3, which in this case appears to be better crystallized. The tetragonal form seems still present, and now small new peaks at 2θ = 31.00 and 36.60° indicate the presence of $NiWO_4$. The formation of $W_{20}O_{58}$, however, is not evident any more.

As we move on to the next atomic ratio (W/Ni = 2), there is still evidence of well-crystallized monoclinic WO_3, together with larger amounts of $NiWO_4$. However, the nickel tungstate peaks were negligible for W/Ni = 1 and completely undetectable for W/Ni = $\frac{1}{2}$ (diffractograms not included in Fig. 2).

The crystal size of the species present in the sample W/Ni = 2 were of the order of 500 Å for $NiWO_4$ and 1500 Å for WO_3, while the sizes of the α-Al_2O_3 crystals are about 10,000 to 15,000 Å.

Finally, for 100% nickel on alumina we can see the presence of NiO in the fresh catalyst and metallic nickel in the spent sample.

In summarizing the X-ray information we can say that WO_3 is better crystallized in the presence of nickel. A similar observation has already been made by Voorhoeve and Stuiver (*6*) for the case of nickel–tungsten sulfides. The $NiWO_4$ crystals appear when excess WO_3 is present, because such species is not detected for W/Ni = $\frac{1}{2}$, as mentioned before, though the magnetic susceptibility indicates its possible formation (*5*). Finally, the sample containing NiO alone is greatly reduced to metallic Ni during the course of the reaction.

Electron Spin Resonance

The electron paramagnetic resonance gave us similar kind of spectra for all the catalysts before the reaction, corresponding to impurities in the alumina support, probably iron, but after several hours on stream the catalysts presented some changes. Thus, the sample containing only nickel (W/Ni = 0) shows a strong absorption band at room temperature (g = 2.17 and ΔH = 1050 G), normally ascribed to the ferromagnetic resonance of metallic nickel. This peak is much smaller in the spent sample with W/Ni = $\frac{1}{4}$ and almost disappears for W/Ni = $\frac{1}{2}$.

A new signal is found in the sample W/Ni = ∞ after use, which decreases as the amount of nickel in the spent samples increases, its relative intensity being 1, 28, 18, 47, and 138 for W/Ni ratios $\frac{1}{2}$, 1, 2, 4, and ∞, respectively. This signal is practically symmetrical, with g = 2.002 and $\Delta H \simeq 4$ G, and it disappears on heating the samples in oxygen at 400°C. Treatment of the spent W/Ni = ∞ catalyst under vacuum also affects this ESR signal in the sense that the intensity increases by outgassing the sample at room temperature, but decreases at higher temperatures particularly in the range 500 to 600°C (Fig. 3). Thus, at 10^{-6} Torr the signal has almost

disappeared at 500°C, but it is necessary to go up to 600°C to obtain the same effect if the pressure is only 10^{-3} Torr. In both cases the sample turns blue.

We have been able to obtain a signal with similar characteristics but smaller intensity by outgassing the fresh W/Ni = ∞ catalyst at 10^{-6} Torr and 350°C for 3 hr. The same result is obtained if this fresh sample is calcined in oxygen at 500°C for 3 hr prior to the vacuum treatment, indicating that the signal is not due to any sort of carbonaceous material on the surface of the catalyst. In connection with these vacuum treatments it is worth mentioning that we have used in all cases a greaseless manifold connected to the diffusion and rotary pumps.

Isolated tungsten ions should not present such a signal, nor does the "blue" oxide of tungsten, which we obtained, for example, by treatment of the W/Ni = ∞ sample with H_2 at 400°C for 3 hr, or heating at 500°C and 10^{-6} Torr for 4 hr.

Although we have no direct proof of the absence of any trace of surface carbon in our spent catalysts, which might also be responsible for the ESR signal at $g = 2.002$, we believe on the basis of all the above information that this signal is due to free electrons as suggested by Alquié-Redon *et al.* (*7*). Schiavello *et al.* (*8*, *9*) have also

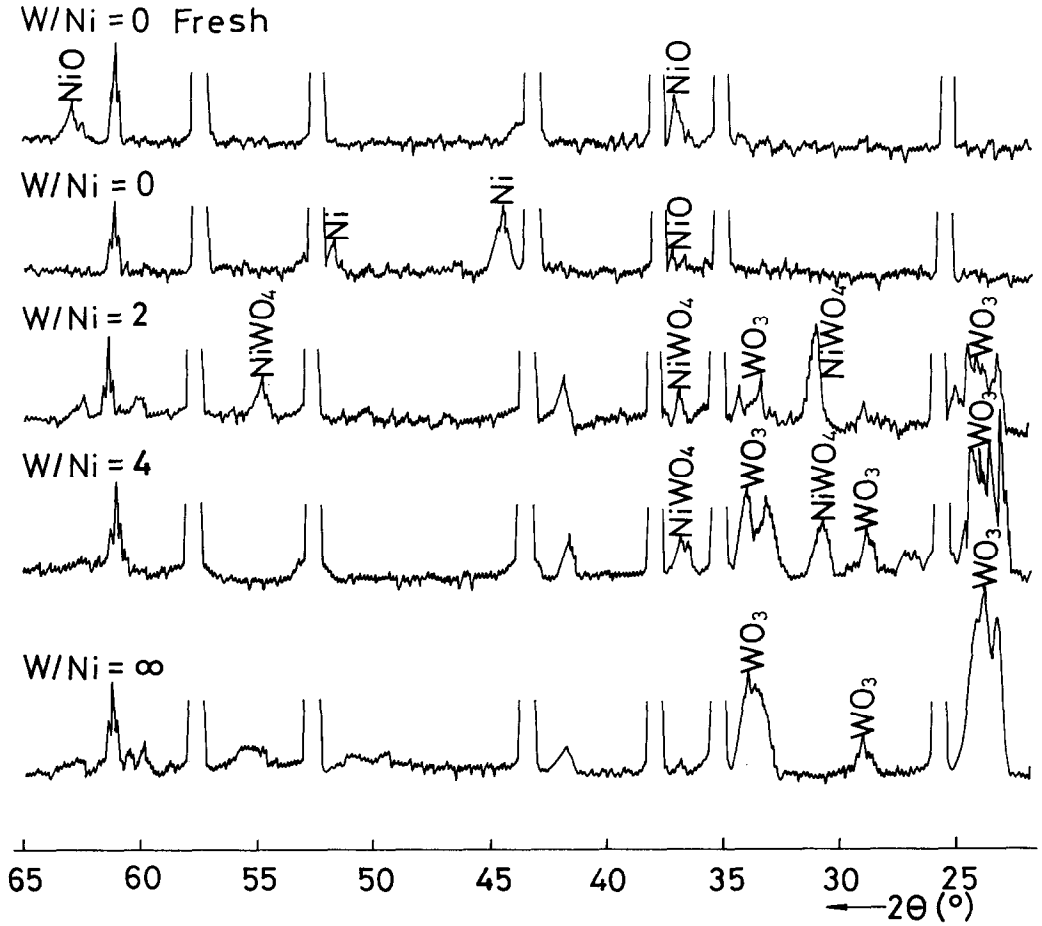

FIG. 2. X-ray diffractograms of the catalyst samples with W/Ni = 0, 2, 4, and ∞.

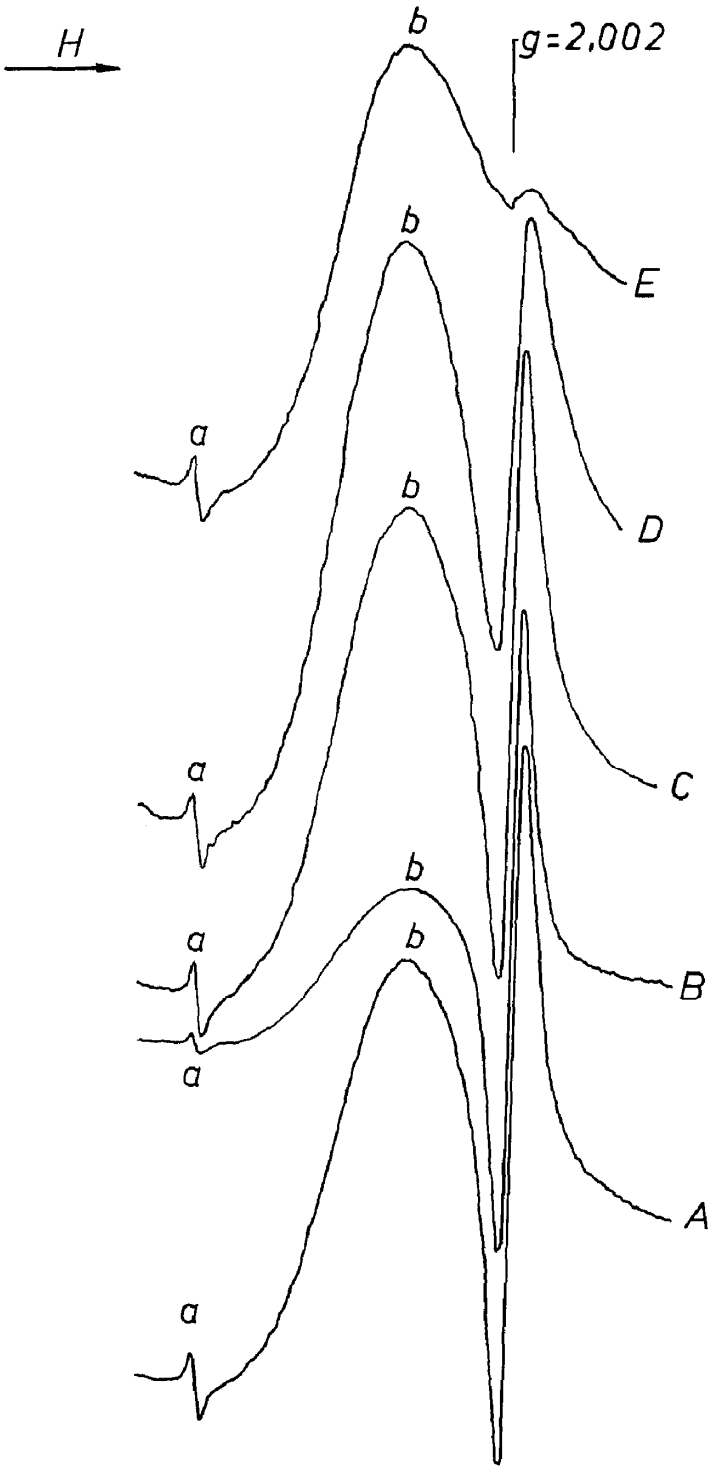

FIG. 3. ESR spectra of the spent W/Ni = ∞ sample: untreated (A) and outgassed at room temperature (B), 200°C (C), 400°C (D), and 500°C (E). Relative intensity of the $g = 2.002$ signal with respect to the manganese external standard (a): 10.1 (A); 30.0 (B); 8.7 (C); 5.5 (D); and 0.4 (E). (b) is an internal impurity of the alumina support.

FIG. 4. Electron diffraction diagram of the spent sample with W/Ni = ∞, showing a long-distance ordered superstructure typical of CS planes in reduced WO_3.

postulated the presence of such free electrons in their high-temperature slightly reduced samples of unsupported WO_3, with the simultaneous formation of crystallographic shear (CS) planes, produced by a change in the bonding of the WO_6 octahedra from a corner to an edge-sharing situation.

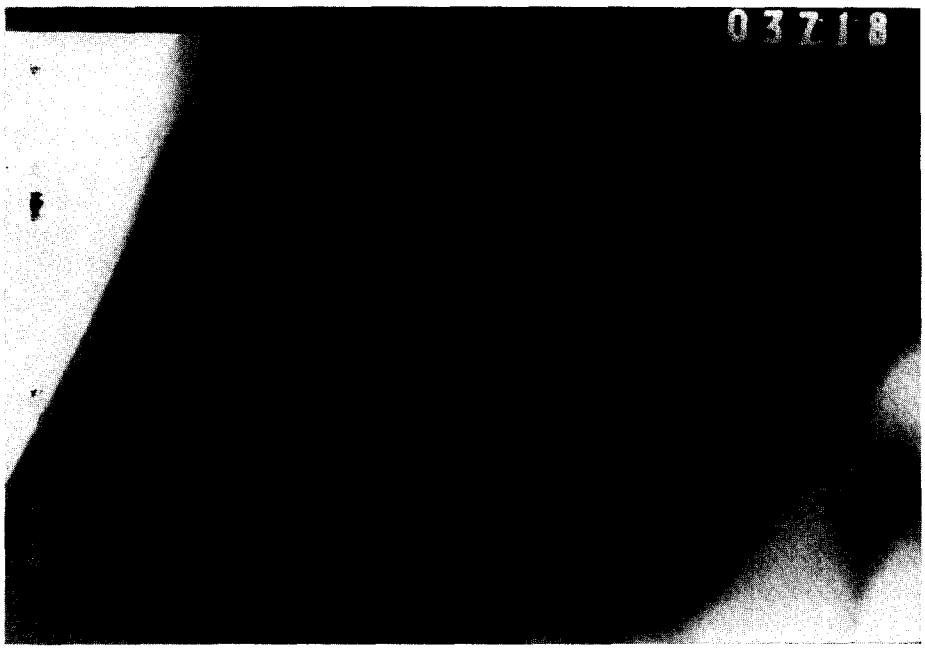

FIG. 5. Transmission electron micrograph (×750,000) of the spent W/Ni = ∞ sample. The defect planes (CS), separated about 20 Å, can best be seen at the edges of the crystal.

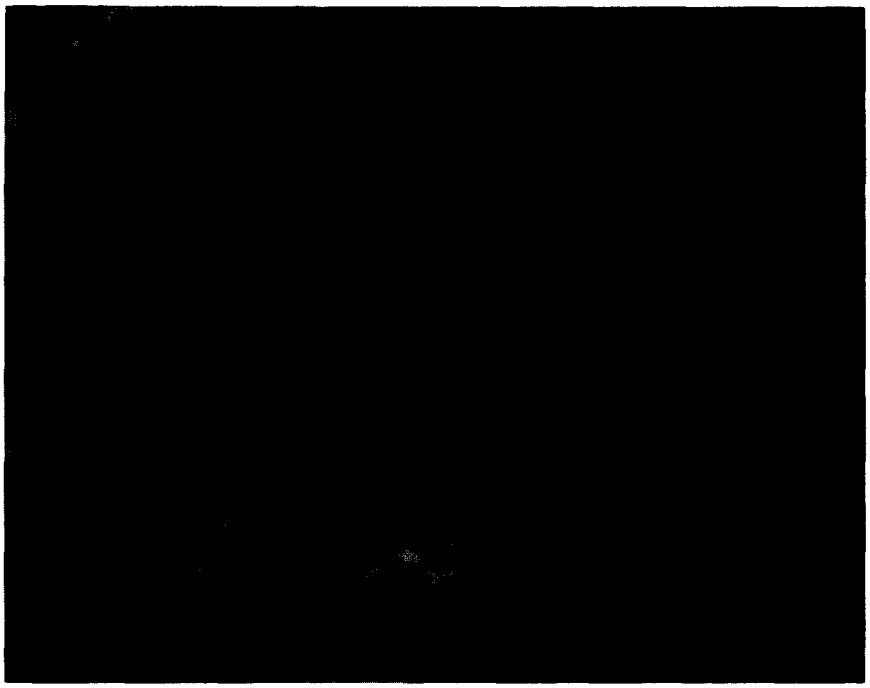

FIG. 6. Scanning electron micrograph (×20,000) of the sample with W/Ni = 4. The large crystals (10,000 to 15,000 Å) are α-Al_2O_3 and the small ones WO_3 (EDAX).

Berak and Sienko (*10*) have indicated that the introduction of CS planes has two effects: (i) to increase the carrier density and (ii) to decrease the carrier mobility. According to these authors, the non-stoichiometric WO_{3-x} consists of two regions: defect and defect-free. In the defect-free region conduction is by band processes, and in the other case fluctuations in composition can replace band states with localized states. The CS planes are characterized by W–W overlap distances considerably smaller than those in normal WO_3 matrix, viz., 3.8 instead of 5.3 Å. Even these W–W distances are not small enough probably for large overlaps of the tungsten $5dt_{2g}$ orbital, but W–W bonds could act as traps for electrons. The XPS data presented by DeAngelis and Schiavello (*11*), indicating that part of the tungsten ions have an electron density corresponding to W^{5+}, is an argument in favor of some sort of localization of the *5d* electrons, so that the ESR signal could also be assigned to trapped electrons, thus explaining the saturation of the signal observed by Alquié-Redon *et al.* (*7*). In any case this signal seems to be related to the formation of CS planes, which we have been able to observe with the transmission electron microscope (Figs. 4 and 5).

The ESR analysis also showed us that pure NiO on α-Al_2O_3 is substantially reduced to nickel metal after several hours of reaction; this reducibility is greatly diminished by the presence of tungsten. Similarly, WO_3 alone on α-Al_2O_3 loses oxygen to a greater extent than when mixed with nickel oxide. The presence of Ni cations, probably in the tunnels of the WO_3 structure (*12*, *13*), appears therefore to lower the oxygen removal by making the WO_3 phase more stable. The degree of reduction of WO_3 in our catalysts, however, is much smaller than that of NiO on α-Al_2O_3, and also unsupported WO_3 (*14*).

Transmission and Scanning Electron Microscopy

The transmission micrographs of Figs. 4 and 5, corresponding to the spent sample with W/Ni = ∞, show the presence of a superstructure characteristic of CS planes in WO_{3-x}.

The fresh catalyst samples containing W/Ni = 0, 2, 4, and ∞ were analyzed with a scanning microscope, equipped with an EDAX accessory, to check the results obtained by X-ray diffraction about the size of the crystals. Figures 6 and 7 show the enlargement of the WO_3 crystals, identified by EDAX, when the amount of nickel increases from W/Ni = 4 to 2.

CONCLUSION

We have shown that the catalyst containing only nickel oxide is mostly reduced to Ni metal during the oxidative dehydrogenation of ethylbenzene. Tungsten oxide on α-alumina, on the other hand, loses small amounts of lattice oxygen, and both oxides are more stable toward reduction in the mixed catalyst samples.

Tungsten trioxide, particularly in the low temperature monoclinic form, shows a better crystallization pattern in the presence of nickel oxide. So also does nickel tungstate when excess tungsten oxide is present in the oxide mixture.

Finally, on the basis of the information presented in this work, and the activity and selectivity data reported earlier (*4*), we believe that in this series of catalysts, nickel tungstate and tungsten trioxide are the species most active and selective toward styrene formation. The maximum in activity and selectivity for W/Ni ratios of 2 to 4 may be interpreted by the formation of a system which reduces both the loss of oxygen under the reaction conditions and

FIG. 7. Scanning electron micrograph (×20,000) of the sample with W/Ni = 2. The large crystals are α-Al_2O_3, while the smaller ones identified by EDAX are WO_3 (~1500 Å) and $NiWO_4$ (~500 Å).

the subsequent appearance of the less active oxygenated species of the lower valences of nickel and tungsten.

REFERENCES

1. Hucknall, D. J., "Selective Oxidation of Hydrocarbons." Academic Press, New York and London, 1974.
2. Skarchenko, V. K., *Int. Chem. Eng.* **9**, 1 (1969).
3. Boutry, P., Courty, Ph., Daumas, J. C., and Montarnal, R., *Bull. Soc. Chim. Fr.*, 4050 (1968).
4. Cortes, A., and Seoane, J. L., *J. Catal.* **34**, 7 (1974).
5. Cortes, A., Seone, J. L., and Soria, J., *Anal. Quim.* **69**, 725 (1973).
6. Voorhoeve, R. J. H., and Stuiver, J. C. M., *J. Catal.* **23**, 236 and 243 (1971).
7. Alquie-Redon, A. M., Aldaz, A., and Lamy, C., *Surface Sci.* **49**, 627 (1975).
8. Schiavello, M., Tilley, R. J. D., De Rossi, S., and Iguchi, E., *Z. Phys. Chem. N.F.* **104**, 165 (1977).
9. De Rossi, S., Iguchi, E., Schiavello, M., and Tilley, R. J. D., *Z. Phys. Chem. N. F.* **103**, 193 (1976).
10. Berak, J. M., and Sienko, M. J., *J. Solid State Chem.* **2**, 109 (1970).
11. De Angelis, B. A., and Schiavello, M., *J. Solid State Chem.* **21**, 67 (1977).
12. Labbe, P., Goreaud, M., Raveau, B., and Monier, J. C., *Acta Crystallogr.* **B34**, 1433 (1978).
13. Magneli, A., *Acta Chem. Scand.* **7**, 315 (1953).
14. Biloen, P., and Pott, G. T., *J. Catal.* **30**, 169 (1973).